Numerical simulation of a turbulent flow in a channel with surface mounted cubes

Verstappen, R.W.C.P.; Veldman, A.E.P.

Published in:
Applied Scientific Research

Publication date:
1998


Applied Scientific Research **59:** 395–408, 1998.

Numerical Simulation of a Turbulent Flow in a Channel with Surface Mounted Cubes

R.W.C.P. VERSTAPPEN and A.E.P. VELDMAN
Department of Mathematics, University of Groningen, P.O. Box 800, 9700 AV Groningen, The Netherlands

Abstract. In this paper we report on a fourth-order, spectro-consistent simulation of a complex turbulent flow. A spatial discretization of a convection-diffusion equation is termed spectro-consistent if the spectral properties of the convective and diffusive operators are preserved, i.e. convection $\leftrightarrow$ skew-symmetric; diffusion $\leftrightarrow$ symmetric positive definite. We consider a fully developed flow in a channel, where a matrix of cubes is placed at a wall of the channel. The Reynolds number (based on the channel width and the mean bulk velocity) is equal to $\mathrm{Re} = 13{,}000$. The three-dimensional flow around the surface mounted cubes has served at a test case at the 6th ERCOFTAC/IAHR/COST workshop on refined flow modeling (Delft, June 1997). Here, mean velocity profiles as well as Reynolds stresses at various locations in the channel have been computed without using any turbulence models. The results agree well with the available experimental data.

AMS Mathematics Subject Classifications (1991): 76F10, 76M25, 65M06.

Key words: direct numerical simulation, turbulent (channel) flow, bluff bodies.

1. Introduction

Kim et al. [1] were among the first who performed numerical simulations of a fully developed channel flow based on the incompressible Navier–Stokes equations without using any turbulence models. The data-base resulting from their simulation has been studied intensively; we mention Mansour et al. [2]. The generally received opinion about simulations that do not use any turbulence models is that these simulations are so computationally expensive that they have to be restricted to simple flows at relatively low Reynolds numbers. In the foreseeable future, however, these limitations will become weaker due to the enormous pace at which the costs of computer simulations go down.

Since a significant part of the reduction of these costs is due to improvements of computational algorithms for fluid flows, it is important to have well-defined test cases so that the algorithmic efficiency of Navier–Stokes solvers can be evaluated regularly. The 6th ERCOFTAC/IAHR/COST workshop on refined flow modeling (Delft, June 1997) offered such a test case: a fully developed flow in a channel, where a matrix of 25×10 cubes is placed regularly at a wall of the channel. The

Reynolds number based on the channel width and the mean bulk velocity is equal to $\mathrm{Re} = 13{,}000$.

Originally, this test case was proposed to evaluate the performance of turbulence models for complex flows. Yet, the complex geometry of this test case makes it also interesting from a computational point of view. Indeed, the pseudo-spectral method (with Fourier-modes in the streamwise and spanwise directions and Chebychev polynomials in the normal direction) that Kim et al. [1] applied to discretize their channel flow cannot be applied here. Thus, other cheap(er) and accurate discretization methods have to be considered. Such methods must be used in combination with nonuniform grids, i.e. stretched grids with high densities of grid points near the walls.

On nonuniform grids various ways exist to discretize convective and diffusive operators. Some examples of higher-order discretization methods can be found in [3–8]. In Section 2, we focus on a fourth-order, spectro-consistent discretization method. In such an approach, the spectral properties of the convective and diffusive operators are preserved, i.e. convection $\leftrightarrow$ skew-symmetric; diffusion $\leftrightarrow$ symmetric positive definite.

We have applied the fourth-order, spectro-consistent discretization of the incompressible Navier–Stokes equations (without any turbulence models) to compute the flow in the channel with an array of surface mounted cubes. Computations have been performed on two different grids. Mean velocities and Reynolds stresses at various locations in the channel are compared to those of RANS computations and to those measured by Meinders et al. [9] (Section 3).

2. Simulation Method

In this section, the main lines of the simulation method are described concisely. Section 2.1 concerns the computational domain and the grid. The time-integration method is discussed in Section 2.2. The spectro-consistent discretization is briefly outlined in Section 2.3. For a more detailed discussion of the numerics the reader is referred to [10].

2.1. Computational domain and grid

We consider the flow in a channel, where a matrix of cubes is placed regularly at one wall of the channel. The matrix consists of 25×10 cubes in the streamwise and the spanwise direction, respectively. The width of the channel is $3.4h$, where h denotes the width of a cube. The pitch of the cubes is $4h$, both in the streamwise and in the spanwise direction. Flow measurements (of Meinders et al. [9]) at the mid height of the channel around a cube at the 18th row from the inlet showed that the influence of the in- and outlet can be neglected there: a fully developed and symmetrical state was observed at this location. This justifies to confine the computational domain to a sub-channel unit of dimension $4h \times 3.4h \times 4h$ with

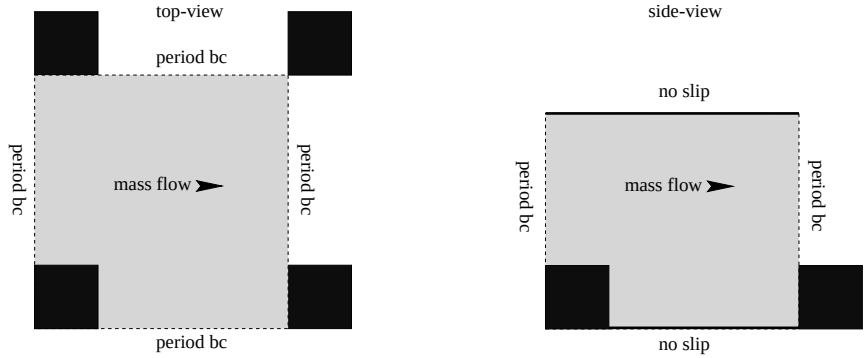

Figure 1. Top- and side-view of the sub-channel unit.

periodic boundary conditions in the streamwise and in the spanwise direction. Figure 1 displays the sub-channel unit. It may be noted that the sub-channel unit may be translated arbitrary in stream- and spanwise direction. We have chosen the sub-channel unit in such way that the computational domain contains only one cube, since this eases the implementation of the boundary conditions in our simulation code. No-slip conditions are imposed at the surfaces of the cubes and at the walls of the channel.

For the Reynolds number considered here, we have computed solutions of the incompressible Navier–Stokes equations on two grids, a coarse grid and a finer grid. The coarse grid uses 60^3 grid points to cover the sub-channel unit; the finer grid has 100^3 grid points. Both grids are staggered and stretched away from the walls using a sinh. This holds for all walls, of the channel as well as of the cubes. For the 60^3-grid, the first grid point away from a wall is located at one hundredth of the channel width. The first mesh point of the 100^3-grid is spaced 40% nearer to the wall. A cube is represented by 20 grid points in each direction on the 60^3-grid, and by 40 grid points on the 100^3-grid. The largest grid size is approximately three (100^3-grid) to four (60^3-grid) times the smallest.

2.2. One-leg time-integration method

The conservation laws for momentum and mass of an incompressible fluid read

$$\frac{\partial}{\partial t}\int_{\Omega} \mathbf{u}\,\mathrm{d}\Omega - \oint_{\partial\Omega} \mathbf{f}(\mathbf{u})\mathbf{n}\,\mathrm{d}s + \oint_{\partial\Omega} p\mathbf{n}\,\mathrm{d}s = \mathbf{0}, \tag{1}$$

$$\oint_{S} \mathbf{u}\cdot\mathbf{n}\,\mathrm{d}s = 0, \tag{2}$$

where Ω is an arbitrary volume with boundary $\partial\Omega$; S is an arbitrary surface; $\mathbf{n}$ denotes the unit normal vector on the surface of integration. The vector $\mathbf{u}$ denotes

the velocity; the scalar p is the pressure. The flux $\mathbf{f}(\mathbf{u})$ consists of a convective and a diffusive part.

The pressure in Equation (1) and the incompressibility constraint (2) are treated implicitly in time to keep the integration method stable. The flux is integrated by means of the following second-order one-leg method

$$\int_{\Omega} \left(\left(\alpha + \frac{1}{2} \right) \mathbf{u}^{n+1} - 2\alpha \mathbf{u}^{n} + \left(\alpha - \frac{1}{2} \right) \mathbf{u}^{n-1} \right) \mathrm{d}\Omega$$

$$- \delta t \oint_{\partial\Omega} \mathbf{f}((1+\alpha)\mathbf{u}^{n} - \alpha \mathbf{u}^{n-1}) \mathbf{n} \, \mathrm{d}s = \mathbf{0}, \tag{3}$$

where we have taken $\alpha = 0.05$ to optimize the (convective) stability of the method [10].

The pressure gradient is added to the solution of Equation (3), where the pressure is solved from a Poisson equation. Here, it may be stressed that the streamwise boundary conditions for the pressure are not periodical, since the mass flow rate through the sub-channel unit is prescribed (such that the Reynolds number is kept constant at Re $=$ 13,000). We satisfy this condition by computing a pressure drop δp, which depends on time, but not on space. To compute the pressure drop without iteration, the pressure p is written as $p = q + s\delta p$, where q satisfies a Poisson equation with periodic boundary conditions in the streamwise direction, and the scalar s satisfies a Laplace equation, where s at the outflow boundary is one unit smaller than s at the inflow. The part q of the pressure is computed every time step, namely in such a way that the divergence of the corresponding, discrete, velocity field is zero; the time-independent part s is computed only once (before the time integration starts). The discrete Poisson equations for q and s are solved numerically using a conjugate gradient method with a modified incomplete Choleski preconditioner.

2.3. Spectro-consistent discretization

On nonuniform grids various ways exist to discretize convective and diffusive operators. This section concerns spectro-consistent discretization methods, i.e. discretizations that preserve the spectral properties of the underlying continuous operators: convection $\leftrightarrow$ skew-symmetric; diffusion $\leftrightarrow$ symmetric positive definite. Both second-order and fourth-order versions are considered. The second-order method can be found in [11]. The fourth-order method follows from a Richardson extrapolation with a second-order discretization applied to a larger-sized grid. Using a doubly-sized grid, the discretization of convection and diffusion becomes (in 1D)

$$h_i \frac{\partial u}{\partial x}_i \approx \frac{1}{2} \left(-u_{i+2} + 8u_{i+1} - 8u_{i-1} + u_{i-2} \right), \tag{4}$$

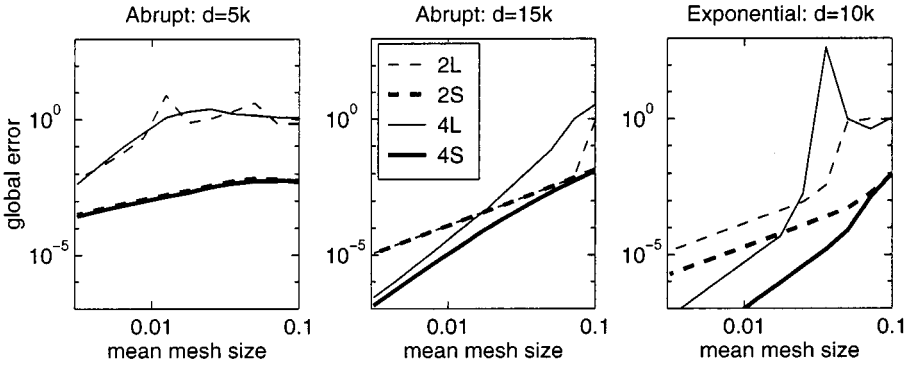

Figure 2. The global error as a function of the mean mesh size.

$$h_i \frac{\partial^2 u}{\partial x^2}_i \approx 8\left(\frac{u_{i+1}-u_i}{x_{i+1}-x_i}-\frac{u_{i-1}-u_i}{x_{i-1}-x_i}\right)-\left(\frac{u_{i+2}-u_i}{x_{i+2}-x_i}-\frac{u_{i-2}-u_i}{x_{i-2}-x_i}\right), \qquad (5)$$

where $h_i = (1/2)\,(-x_{i+2} + 8x_{i+1} - 8x_{i-1} + x_{i-2})$.

On a uniform grid we obtain the usual fourth-order method, but on nonuniform grids the method differs. It is easy to show that, in the absence of diffusion, this method conserves quadratic quantities.

Figure 2 shows a comparison of the fourth-order spectro-consistent method (4–5) with the traditional discretization methods. For this comparison, an exact solution of the following steady, one-dimensional convection-diffusion equation with a boundary-layer character has been considered:

$$\frac{\partial u}{\partial x} - k\frac{\partial^2 u}{\partial x^2} = 0 \quad (0 < x < 1) \quad u(0) = 0, \quad u(1) = 1. \qquad (6)$$

The diffusion coefficient is equal to $k = 0.001$. Two types of grids have been examined: piecewise-uniform grids (which consist of two parts, in each of which the grid is taken uniform) and exponentially stretched grids. In both cases half of the grid points are located in a layer with thickness $d = O(k)$. Four discretization methods have been investigated: (2L) the traditional Lagrangian second-order method; (2S) the second-order spectro-consistent method; (4L) the traditional fourth-order Lagrangian method where we have implemented exact boundary conditions to circumvent the problem of the difference molecule that is too large near the boundary; (4S) the method defined by Equations (4–5) where the problems due to the 'missing' boundary conditions are solved by using the second-order discretization in the end points.

The numerical experiments with the four discretization methods show that often the fourth-order Lagrangian method is not more accurate than its second-order counterpart, especially when the number of grid points is not abundant. Further, when the number of grid points is low Lagrangian discretization is much less accurate than spectro-consistent discretization. Though the local order of 2S and

4S is only one at the grid-transition point of the abrupt grids, the global error of 2S and 4S is smaller than that of the Lagrangian methods 2L and 4L. As can be seen in Figure 2, the spectro-consistent discretization method behaves smoothly on all grids. In contrast, the fourth-order Lagrangian method nearly breaks down on the exponential grid if the stretching factor is 0.72 (which is not extreme; for this stretching factor 4S is already very accurate, with an error around 10^{-5}). This bad result of the Lagrangian method 4L is due to an eigenvalue crossing the imaginary axis close to the origin. For a mean grid size of 0.1 some eigenvalues of the coefficient matrix of both 2L and 4L are located in the unstable halfplane. Upon grid-refinement some of these eigenvalues will cross the imaginary axis. If they do so close to the origin, the discrete system is (almost) singular, and consequently, the global truncation error – which is the product of the inverse of the coefficient matrix and the local truncation error – may become large. This cannot happen with a spectro-consistent discretization, since in such an approach all eigenvalues lie where they belong: in the stable halfplane.

The above ideas have been implemented in a simulation method for solving the incompressible Navier–Stokes equations in three spatial dimensions. To this end, the Navier–Stokes equations are discretized on a staggered grid, where the velocities and pressure are defined on the grid as proposed by Harlow and Welsh [12]. The spatial integrations in the time-discrete momentum equation (3) are approximated by means of the midpoint rule. The leading term of the local truncation error of the approximation consists of second-order terms. To eliminate the leading term of the truncation error, the momentum equations are also integrated over three times larger control volumes. On a staggered grid we have to use three times larger control volumes, and not two times larger as in Equations (4–5), since three times larger volumes are the smallest ones possible that have exactly the same properties as the original volumes.

For more details about the fourth-order spectro-consistent method, we refer to [10]. In that paper, we have also compared the results of the fourth-order spectro-consistent method and the underlying second-order method for a direct numerical simulation of the flow in a cubical lid-driven cavity at $\mathrm{Re} = 10{,}000$. In this example, the fourth-order results are clearly superior to the second-order results, whereas the computational effort is about 20 times less.

3. Results and Discussion

We have applied the fourth-order, spectro-consistent method that is outlined in the previous section to compute mean velocity profiles as well as Reynolds stresses at various locations in a sub-unit of a channel with surface mounted cubical obstacles. The distance between the walls of the channel is 3.4 times the length of a cube. The pitch of the cubes is four cube lengths in both the streamwise and the spanwise direction. The Reynolds number based on the width of the channel and the bulk velocity is equal to $\mathrm{Re} = 13{,}000$.

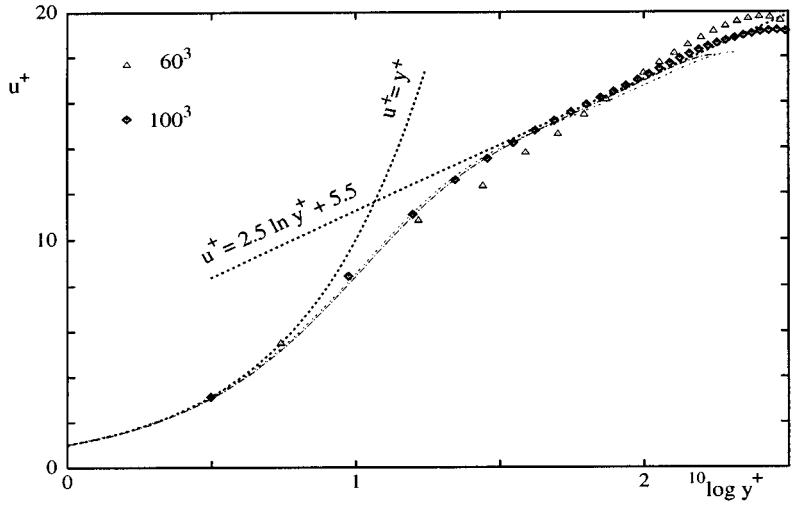

Figure 3. Comparison of the mean streamwise velocity near the flat wall of the channel. Here, the profiles of the mean velocity are nondimensionalized by the wall-shear velocity. The distance to the wall is measured in wall coordinates. The doted lines represent the law of the wall and the log law. The markers correspond to the 60^3 and 100^3 simulation; the dashed lines are taken from the ERCOFTAC Database (short dashes: DNS of Kim et al. [1]) and from the Japanese DNS Data Base of Turbulent Transport Phenomena (DNS of Gilbert and Kleiser [13]).

The initial velocity field is taken constant ($u = 1$, $v = w = 0$). The sampling of data for the computation of the first- and second-order statistics of the flow started after a transitional period of 100 time units (nondimensionalized by the bulk velocity and the channel width). All averages have been computed over 200 nondimensional time units and over the two symmetrical halves of the sub-channel unit. Samples have been taken at each time step.

3.1. How accurate is the 60^3 simulation compared to 100^3?

The flow has been simulated at two grids; see Section 2.1. Including start-up and sampling time, the 100^3 simulation took about 100 hours on one vector-processor of a CRAY C90. The 60^3 simulation took about one tenth of the CPU-time of the 100^3-simulation. Half of this reduction results from a doubling of the time step (which is restricted by the CFL-condition).

Figure 3 displays a comparison between the mean streamwise velocities near the flat wall of the channel of the fine grid simulation, the coarse grid simulation, the DNS of Kim et al. [1] and the DNS of Gilbert and Kleiser [13]. The latter two are added for comparison. It may be noted that the flow conditions are not exactly equal: Kim et al. and Gilbert and Kleiser have considered a turbulent channel flow

without surface-mounted cubes. Their Reynolds numbers are 5,600 and 6,600, respectively.

Here, it may be remarked that the u^+ of 60^3 and 100^3 simulations are obtained by averaging over the time and the streamwise direction, but not over the spanwise direction since the data needed for that was not stored during the simulations. Therefore, the mean-velocity profiles are computed at the cross section that bisects the cubes.

The markers in Figure 3 indicate the computed values at the 60^3 and 100^3 grid. The first grid point of the 60^3 is located at $y^+ = 5.490982$; the first grid point of the 100^3 grid lies at $y^+ = 3.140607$. Hence, the first grid point of the coarse grid lies just outside the viscous sublayer ($y^+ < 5$), while the 100^3 grid has only one grid point inside. Yet, all computational results follow the the linear law of the wall in the sublayer: the computed values of u^+ at the first grid point of the 60^3 and 100^3 grid are 5.490982 and 3.140607, respectively.

In the logarithmic layer, however, the results on the two grids differ significantly. The 60^3 simulation does not follow the log law, while the fine grid simulation (like the DNSs of Kim et al. and Gilbert and Kleiser) follows the log law, where we have used 5.5 for the additive constant instead of 5 to compensate for the relatively low Reynolds number (see also [1] and [14]). From this it is clear that the 60^3 grid is not fine enough to capture all the details of the flow near the flat wall of the channel. One of the main shortages of the 60^3 simulation seems to be the misprediction of the wall-shear velocity that is used to scale the velocity profiles. Using the wall-shear velocity of the 100^3 simulation to scale the velocities of the 60^3 simulation improves the results somewhat, yet not enough to approximate the log law with an error smaller than 5%.

It may noted that the DNS of Kim et al. [1] and the DNS of Gilbert and Kleiser [13] use a much finer grid near the wall than we do. Both Kim et al. and Gilbert and Kleiser use approximately 10 grid points to cover the viscous sublayer, while the 100^3 grid has only one grid point inside the viscous sublayer. Nevertheless, the values of the mean velocities and the turbulence intensities of the 100^3 simulation agree well with the available experimental data. The computed value of the root-mean-square of the fluctuating streamwise velocity u_{rms} near the wall, for example, equals 0.31 (normalized by the mean streamwise velocity $\overline{u}$); the experimental results reported in [15] lie in the range 0.3–0.32. The experiments show that $u_{\mathrm{rms}}/\overline{u}$ is almost constant in the viscous sublayer.

Next, we will consider the flow in a cross section of the channel with surface mounted cubical obstacles. Here, all quantities are normalized by the channel width and the bulk velocity. The mean-square of the fluctuating spanwise velocity of the fine grid simulation, the coarse grid simulation and the experiments of Meinders et al. [9] are shown in Figure 4. As can be seen in Figure 4, the 100^3 simulation predicts the mean-square of the fluctuating velocity correct, while the 60^3 simulation is far off. It predicts the extremal values of the mean-square of the fluctuating velocity wrong. The peak of $\overline{w'w'}$ near the cube of the 60^3 simulation is approximately 70%

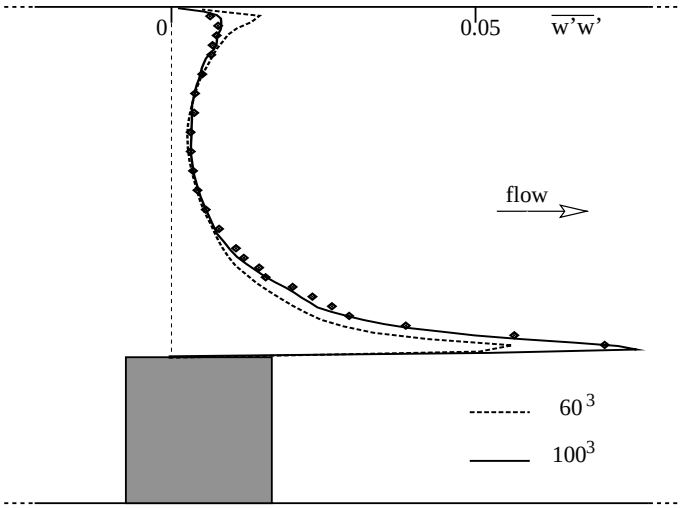

Figure 4. A comparison of the mean-square of the fluctuating spanwise velocity at a cross section of the channel. The cross section is taken perpendicular to the spanwise direction and bisects the cube. The geometry is drawn to scale. The continuous line corresponds to the 100^3 simulation; the dashed line denotes the 60^3 result; the experimental data is depicted by the dots.

of that of the 100^3 simulation. The peak near the flat wall of the channel is about 100% larger than that of the 100^3 simulation.

So, in conclusion, the 60^3 simulation cannot compete with the 100^3 simulation in terms of accuracy.

3.2. COMPARISON WITH RANS

We have merely pursued the 60^3 simulation to challenge Reynolds-averaged Navier–Stokes (RANS) computations, not to challenge DNS. We think that a RANS computation of this flow has to be performed on a grid that is comparable to the 60^3 grid in order to represent the geometry sufficiently accurate. Here, it may be recalled that a cube is represented by as little as 20 grid points in each direction on the 60^3 grid. Thus, regarding the spatial resolution a 60^3 computation of Navier–Stokes without using any turbulence models may challenge RANS. In fairness it must be said that this does not necessarily hold with regard to the temporal resolution, since a RANS computation need not to be time-accurate, while our 60^3 simulation is time-accurate.

The flow in the channel with surface mounted cube was one of the test cases at the 6th ERCOFTAC/IAHR/COST Workshop on Refined Flow Modelling (Delft, June 1997). There were four groups who presented results of their RANS computations of the flow in the channel with surface mounted cubes. Here, we restrict ourselves to the submission (of Dr. S. Jansson from the Department of Fluid Me-

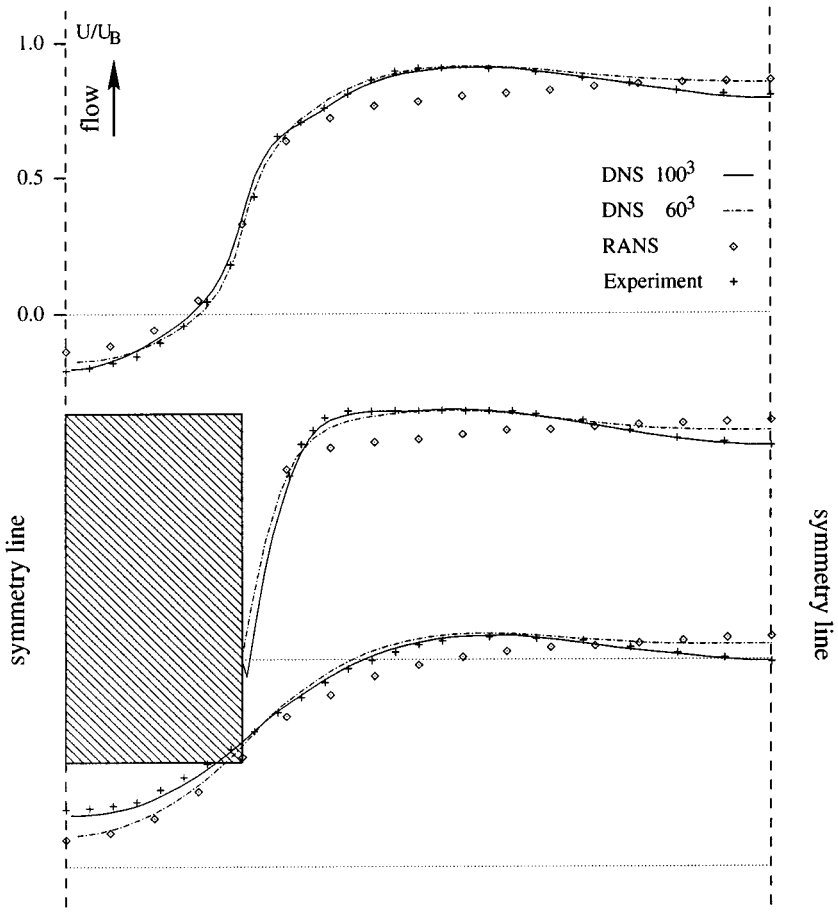

Figure 5. Comparison of the mean streamwise velocity at half cube height. The flow comes from below. The horizontal corresponds to the spanwise direction. The dashed vertical lines are lines of symmetry. The distance between them is two cube lengths. The lowermost profiles are located at 0.3 cube lengths before the front of the cube; the middlemost profiles are located at 0.3 cube lengths after the front. The uppermost profiles are located at one cube length after the middlemost. The velocity scale is shown for the uppermost profiles only; the other profiles have the same vertical scale. All velocities are normalized by the bulk velocity.

chanics of Vattenfall Entvecklung AB in Sweden) that, among the RANS, agreed the best with the available experimental data. This RANS computation was performed on a stretched, orthogonal grid of 67 by 72 by 57 points in the streamwise, the normal and the spanwise direction, respectively. The grid points that are located closest to a wall were taken at $y^+ = 2$–5. The results of this RANS as well as those of all the other submitted computations can be found in the proceedings of the workshop [16]. It may be noted that there were no results of large-eddy simulations submitted to this workshop, nor have there been any reported elsewhere.

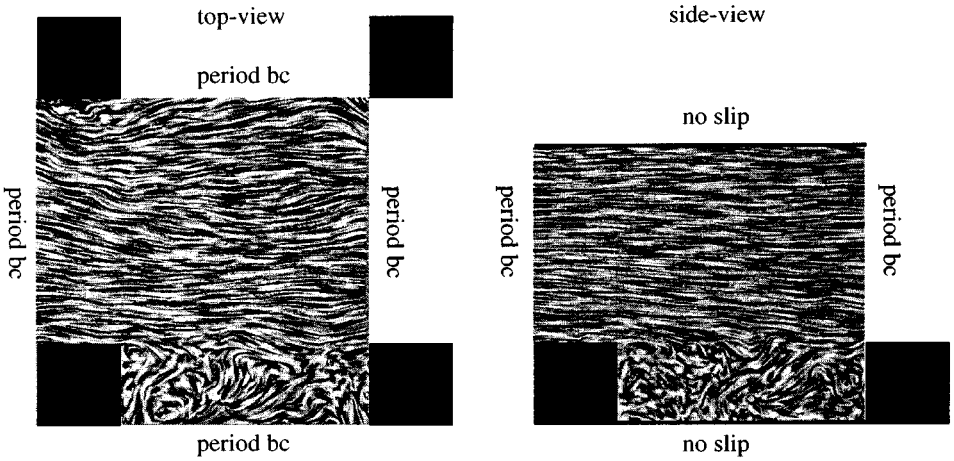

Figure 6. An instantaneous flow field at two planes through the centre of the cubes. In both pictures the flow is directed from left to right.

The best RANS result was based on a second-order, cell-centred, finite-volume method. It applied the SIMPLEC solution technique and a Rhie and Chow interpolation method. The QUICK scheme was used for the velocities and the turbulent quantities were integrated by means of a second-order accurate scheme with a Van Leer limiter. Periodic boundary conditions were applied in the streamwise direction; the period was taken equal to four cube lengths. Symmetry conditions were applied in the spanwise directions. The spanwise boundaries were taken two cube lengths apart. Dirichlet conditions were applied at the solid walls, except for the dissipation rate ε: the normal derivative of ε was put to zero at solid walls. The turbulence model consisted of a two-layer eddy-viscosity combined with a standard k–ε model. The transport equation for the dissipation rate ε was not solved in near-wall regions, but instead it was computed explicitly from a predicted length scale.

Mean streamwise velocity of the best RANS computation are compared to those of the 60^3 and the 100^3 Navier–Stokes computation in Figure 5. Here, the experimental data of Meinders et al. [9] forms the frame of reference. On a corresponding grid, the mean velocities computed from the Reynolds averaged Navier–Stokes equations agree less with the experimental data than the results of the 60^3 Navier–Stokes computation. The velocity profiles of the RANS computation are much too smooth. In addition, the maxima of the velocities are located in the symmetry-plane between two cubes, which is in distinct disagreement with the experimental data.

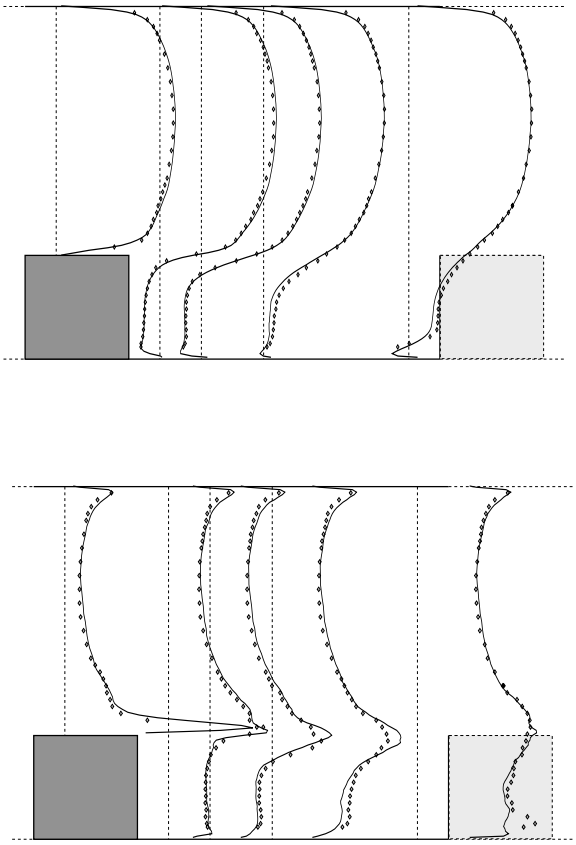

Figure 7. A comparison of first-order statistics (upper picture) and second-order statistics (lower picture) of the DNS with experimental data. Shown are the mean streamwise velocity $\overline{u}$ (upper picture) and $\overline{u'u'}$ (lower picture) in the plane parallel to the streamwise direction that cuts the cubes in two equal halfs. The continuous lines correspond to the DNS; the experimental data is depicted by the dots.

3.3. MORE RESULTS OF THE 100^3 SIMULATION

From the previous two sections it is obvious that the results of the 100^3 simulation are closer to the measurements than those of the 60^3 simulation. Therefore, we will focus on the 100^3 simulation in this final section.

Figure 6 shows an instantaneous flow field. The visualization has been made by means of the spot noise technique. For details on this technique the reader is referred to [17]. It may be noted that large structures of recirculating flow behind the cubes are not present in Figure 6, nor have they been observed in any of the snapshots of this flow. These regions can only be seen if the flow is averaged over a long period in time.

First- and second-order statistics of the flow at the cross section of the channel that bisects a cube are compared to experimental data of Meinders et al. [9] in

Figure 7. As before, the averages are computed over 200 (nondimensional) time units. The profiles are also averaged over the two symmetrical halves of the computational domain. The profiles of the mean streamwise velocity and the mean-square of the fluctuating streamwise velocity are in good agreement with the experiments, except in front of a cube, where some discrepancies between the mean-squares of the fluctuating streamwise velocities exists.

Acknowledgement

The Stichting Nationale Computerfaciliteiten (National Computing Facilities Foundation, NCF) with financial support from the Nederlandse Organisatie voor Wetenschappelijk Onderzoek (Netherlands Organization for Scientific Research, NWO) is gratefully acknowledged for the use of supercomputer facilities.

References

1. Kim, J., Moin, P. and Moser, R., Turbulence statistics in fully developed channel flow at low Reynolds number. *J. of Fluid Mech.* **177** (1987) 133–166.
2. Mansour, N.N., Kim, J. and Moin, P., Reynolds-stress and dissipation-rate budgets in a turbulent channel flow. *J. of Fluid Mech.* **194** (1988) 15–44.
3. Fasel, H.F., Numerical simulation of instability and transition in boundary layer flows. In: Arnal, D. and Michel, R. (eds), *Laminar-Turbulent Transition*. Springer-Verlag, Berlin (1990) pp. 303–308.
4. Rai, M.M. and Moin, P., Direct simulations of turbulent flow using finite-difference schemes. *J. Comp. Phys.* **96** (1991) 15–53.
5. Joslin, R.D., Streett, C.L. and Chang, C.L., Validation of three-dimensional incompressible spatial direct numerical simulation code – A comparison with linear theory and parabolic stability equation theories for boundary layer transition on a flat plate. NASA Technical Paper 3205 (1992).
6. Lele, S.K., Compact finite difference schemes with spectral-like resolution. *J. Comp. Phys.* **103** (1992) 16–42.
7. Liu, Z. and Liu, C., Fourth order finite difference and multigrid methods for modeling instabilities in flat plate boundary layers – 2D and 3D approaches. *Comput. & Fluids* **7** (1994) 955–982.
8. Kravchenko, A.G., Moin, P. and Moser, R., Zonal embedded grids for numerical simulation of wall-bounded turbulent flows. *J. Comp. Phys.* **127** (1996) 412–423.
9. Meinders, E.M., Hanjalić, K., Obi, S. and van der Meer, T., The flow in a matrix of cubical protrusions placed in a fully developed low Re number channel flow. Submitted.
10. Verstappen, R.W.C.P. and Veldman, A.E.P., Direct numerical simulation of turbulence at lower costs. *J. Engrg. Math.* **32** (1997) 143–159.
11. Veldman, A.E.P. and Rinzema, K., Playing with nonuniform grids. *J. Engrg. Math.* **26** (1992) 119–130.
12. Harlow, F.H. and Welsh, J.E., Numerical calculation of time-dependent viscous incompressible flow of fluid with free surface. *Phys. Fluids* **8** (1965) 2182–2189.
13. Gilbert, N. and Kleiser, L., Turbulence model testing with the aid of direct numerical simulation results. In: *Proc. of 8th Symposium on Turbulent Shear Flows*, Paper 26-1, Munich, September 9–11 (1991).

14. Johansson, A.V. and Alfredsson, P.H., On the structure of turbulent channel flow. *J. Fluid Mech.* **122** (1982) 295–314.
15. Hanratty, T.J., Chorn, L.G. and Hatziavramidis, D.T., Turbulent fluctuations in the viscous wall region for Newtonian and drag reducing fluids. *Phys. Fluids* **20** (1977) S112–S119.
16. Hanjalić, K. and Obi, S. (eds), *Proceedings 6th ERCOFTAC/IAHR/COST Workshop on Refined Flow Modeling*, Vol. 3, Delft University of Technology, Delft, The Netherlands (1997).
17. Leeuw, W. de, Presentation and exploration of flow data. Ph.D. Thesis, Technical University of Delft, Delft, The Netherlands (1997).